Available online at www.sciencedirect.com

ScienceDirect

www.elsevier.com/locate/jes

JES JOURNAL OF ENVIRONMENTAL SCIENCES

www.jesc.ac.cn

Surface-enhanced Raman scattering for mixing state characterization of individual fine particles during a haze episode in Beijing, China

Hui Chen[1], *Fengkui Duan*[2], *Jingjing Du*[3], *Ranhao Yin*[4], *Lidan Zhu*[2], *Jinlu Dong*[2], *Kebin He*[2], *Zhenli Sun*[1,*], *Suhua Wang*[1,4]

[1] *MOE Key Laboratory of Resources and Environmental System Optimization, College of Environmental Science and Engineering, North China Electric Power University, Beijing 102206, China*

[2] *State Key Joint Laboratory of Environment Simulation and Pollution Control, School of Environment, Tsinghua University, Beijing 100084, China*

[3] *State Key Laboratory of Environmental Chemistry and Ecotoxicology, Research Center for Eco-Environmental Sciences, Chinese Academy of Sciences, Beijing 100085, China*

[4] *Guangdong Provincial Key Laboratory of Petrochemcial Pollution Processes and Control, School of Environmental Science and Engineering, Guangdong University of Petrochemical Technology, Maoming 525000, China*

ARTICLE INFO

Article history:
Received 5 October 2020
Revised 4 December 2020
Accepted 8 December 2020
Available online 22 December 2020

Keywords:
$PM_{2.5}$
Surface-enhanced Raman scattering
Individual fine particle
Nitrate
Sulfate
Soot

ABSTRACT

The nondestructive characterization of the mixing state of individual fine particles using the traditional single particle analysis technique remains a challenge. In this study, fine particles were collected during haze events under different pollution levels from September 5 to 11 2017 in Beijing, China. A nondestructive surface-enhanced Raman scattering (SERS) technique was employed to investigate the morphology, chemical composition, and mixing state of the multiple components in the individual fine particles. Optical image and SERS spectral analysis results show that soot existing in the form of opaque material was predominant during clear periods ($PM_{2.5} \leq 75$ μg/m^3). During polluted periods ($PM_{2.5} > 75$ μg/m^3), opaque particles mixed with transparent particles (nitrates and sulfates) were generally observed. Direct classical least squares analysis further identified the relative abundances of the three major components of the single particles: soot (69.18%), nitrates (28.71%), and sulfates (2.11%). A negative correlation was observed between the abundance of soot and the mass concentration of $PM_{2.5}$. Furthermore, mapping analysis revealed that on hazy days, $PM_{2.5}$ existed as a core-shell structure with soot surrounded by nitrates and sulfates. This mixing state analysis method for individual $PM_{2.5}$ particles provides information regarding chemical composition and haze formation mechanisms, and has the potential to facilitate the formulation of haze prevention and control policies.

* Corresponding author.
E-mail: sunliva@ncepu.edu.cn (Z. Sun).

https://doi.org/10.1016/j.jes.2020.12.008
1001-0742/

Introduction

Regional haze episodes have occurred frequently in East Asia in recent years and attract significant research interest (Fu and Chen, 2017; Tan et al., 2009; Wang et al., 2014; Zhuang et al., 2014). Haze episodes have direct and indirect negative impacts on human health and climate change (Kulmala, 2015; Zhang et al., 2015). The effects of haze depend on the physical and chemical properties of the individual $PM_{2.5}$ particles, which are affected by the relative abundances and mixing states of their different components. Studies indicate that the most abundant components of these particles are soot and secondary matter, including secondary inorganic aerosols (SNA, which mainly include sulfates, nitrates, and ammonia salts) and secondary organic aerosols (SOA, which form from primary pollutants, SO_2, NOx, and volatile organic compounds) (Li et al., 2014a; Lu et al., 2015; Wang et al., 2018). Owing to the universality of atmospheric aging and the diversity of pollution sources, $PM_{2.5}$ particles usually exist as internal mixtures of multiple components, and interactions within particles further change their original properties (Li et al., 2014b; Riemer et al., 2019). In previous studies, bulk techniques have predominantly been applied for haze analysis to obtain the mass concentrations of various types of aerosols (Guo et al., 2014; Wang et al., 2009). Although these data can enhance understanding of emission sources and climate impact, they cannot provide specific information about the single particle mixing state.

More advanced methods have been developed for single particle analysis. These include electronic spectroscopy (e.g., transmission electron microscopy [TEM] and scanning electron microscopy [SEM]) and vibrational spectroscopy (e.g., Raman scattering and surface-enhanced Raman scattering [SERS]) (Ault and Axson, 2017; Li et al., 2016a). TEM and SEM both offer high resolution and high magnification particle morphological observations. However, owing to their operation under vacuum conditions, they cause the loss of volatile and semi-volatile components (e.g., sulfates and nitrates), leading to decreased accuracy of analysis results (Li et al., 2013). SERS is an optimized Raman scattering technique; therefore, it is advantageous in that the samples are not destroyed, which can maximize the integrity of the particle components and reveal more persuasive information about mixing state. Furthermore, owing to the chemical enhancement and electromagnetic field enhancement on the surface of the precious metal substrate, SERS can achieve an order-of-magnitude increase in the detection signal, and can detect trace substances in the atmosphere of single particles (Dong et al., 2019; Sun et al., 2019a). Previous studies had established highly sensitive particle identification methods for practical applications using the SERS technique. Minutolo et al. (2011) used SERS to perform spectral characterization of soot particles with three C/O ratios in the flame process. Craig et al. (2015) was the first to use SERS to directly detect trace organic and inorganic substances in atmospheric aerosols, and to observed differences in the SOA components of different particles. Fu et al. (2017) used a commercial substrate Klarite as the SERS substrate; its inverted pyramid structure can achieve laser concentration and convenient sample collection, realizing the portable detection of sulfate and naphthalene. However, these studies on haze particles mostly focused on component identification, without a thorough analysis of the mixing state during haze episode.

The aim of this study was to investigate the morphology, chemical composition, and mixing state of the multiple components in ambient particles using the SERS strategy during real haze episodes. Measurements were made during a particulate matter pollution event that occurred in Beijing from September 5 to 11 2017. Spectral analysis and direct classical least squared (DCLS) analysis of the SERS off-line data combined with on-line observation data revealed the major chemical components of the fine particles and their relative abundances during the haze episode. Mapping analysis successfully showed a distinct type of mixing state of the fine particles during the haze days. These results provide a reference for haze prevention and control.

1. Materials and methods

1.1. Sampling site description and fine particle collection

Beijing, the capital city of China, is severely affected by haze pollution in Autumn and Winter (Yang et al., 2020). Online hourly ambient observations were conducted from September 5 to 11 2017 at a sampling site on the campus of Tsinghua University, Beijing (116.33°E, 40.01°N) (He et al., 2001). The site is approximately 15 m above ground level and can represent an urban environment in Beijing according to our previous study (Xu et al., 2017). Online mass concentration of $PM_{2.5}$ were measured with a PM-712 monitor (Kimoto Electric Co., Ltd., Japan) based on the β-ray absorption method. The hourly average mass concentrations of water-soluble inorganic ions (NO_3^-, SO_4^{2-}) in the online $PM_{2.5}$ were measured using an ACSA-08 monitor (Kimoto Electric Co., Ltd., Japan). Relative humidity (RH), temperature (T), pressure (P), wind speed (WS), and wind direction (WD) were obtained simultaneously using a WXT monitor (Kimoto Electric Co., Ltd., Japan).

For individual fine particle collection, the mass concentration of $PM_{2.5}$ for haze trend analysis and sample collection time were selected according to the Air Quality Index (AQI) observed at the Olympic Center Station in Beijing (http://www.aqistudy.cn). The Dekati Low Pressure Impactor (DLPI) instrument was operated at a flow rate of 10 L/min. The DLPI has 13 stages and a backup filter, and the particle aerodynamic diameter of the stage was 1.6–2.5 μm. Commercial impaction films with a diameter of 2.2 cm were used (Ag foils 10 μm-thick, Nanjing Company, China).

1.2. Materials and SERS analysis

All reagents were of analytical grade and were used without further purification. Standard $(NH_4)_2SO_4$ (AS), NH_4NO_3 (AN), and graphene oxide (GO) were purchased from Sinopharm Chemical Reagent Co., Ltd (China).

For the micro-Raman analysis, an inVia^{TM} Renishaw confocal Raman micro-spectrometer (Renishaw, Gloucestershire, UK) coupled with a Leica microscope was used. Excitation

lasers (633 nm, nominal laser power 7 mW, diffraction grating 1800 l/mm) and a magnification lens (100 × , 0.85 Numerical Aperture) were used to perform the measurements. Data acquisition and analysis were carried out using the WiRE 3.4 software package for SERS analysis. Between 24 and 104 effective spectra for each sample on the Ag foil of the 1.6–2.5 μm stage were randomly selected to conduct spectral, quantity abundance, and DCLS analyses to obtain more comprehensive information on the composition of the fine particles. In quantity abundance analysis, the relative abundance of the $PM_{2.5}$ component was calculated as by Eq. (1):

$$R_A = (N_A/N_T) \times 100\% \quad (1)$$

where, N_A is the number of spectra containing component A, and N_T is the number of total spectra. DCLS is a robust mathematical method of curve fitting that is applied in Raman analysis (Liu et al., 2017b; Vajna et al., 2010). By integrating DCLS into the WiRE software and inputting the known reference spectra, we can fit the unknown spectrum into a linear combination of known reference spectra. The results not only image the specified area, but also provide semi-quantitative compositional information of the reference spectra in the imaging area. The mapping scanning acquisition of fine particles for clear and hazy weather were chosen and analyzed at a 0.5 μm step.

2. Results and discussion

2.1. Haze event overview

A haze event was observed from September 5 to 11 2017; the related air quality parameters are shown in Table 1. According to the Ambient Air Quality Standard (HJ 633-2012), our sampling period was divided into four levels: clear ($PM_{2.5} \leq 75$ μg/m^3, no pollution, green in Fig. 1), lightly polluted (75 μg/m^3 < $PM_{2.5} \leq 115$ μg/m^3, orange in Fig. 1), moderately polluted (115 μg/m^3 < $PM_{2.5} \leq 150$ μg/m^3, red in Fig. 1), and heavily polluted (150 μg/m^3 < $PM_{2.5} \leq 250$ μg/m^3, purple in Fig. 1). During this event, $PM_{2.5}$ varied from 3 to 164 μg/m^3, with 39.05% of the samples indicating that the $PM_{2.5}$ concentration exceeded the daily threshold (75 μg/m^3). On hazy days, the $PM_{2.5}$ concentration was 85.6 times greater than that observed on clear days. The average values of RH and T were 51.5% and 25.9°C, respectively; they varied reversely between day and night. Moreover, hazy days were always accompanied by higher RH and lower WS.

To investigate the mixing state of the fine particles during the haze event, 12 off-line $PM_{2.5}$ particle samples were collected from clear to moderately polluted days over the study period (Fig. 1, six samples on clear days, two on lightly polluted days, and four on moderately polluted days). The relative parameters of the 12 samples are shown in Table 1. Of all the parameters, the $PM_{2.5}$ concentration is the most important because it is indicative of the degree of haze pollution. From samples 1 to 3, pollution became worse as the $PM_{2.5}$ mass concentration increased from 3 to 116 μg/m^{-3}. In samples 3 to 6, the $PM_{2.5}$ mass concentration exceeded 115 μg/m^3, indicating moderate pollution, while samples 7 and 8 showed light pollution (97 and 105 μg/m^3, respectively). Then, the haze dissipated gradually and the air quality index level reverted to "good" until sample 12. The average $PM_{2.5}$ mass concentration was 114.67 μg/m^3 on hazy days, which was 4.5 times higher than the average values before and after the haze event (25.5 μg/m^3; Table 1).

2.2. Single-particle composition analysis

2.2.1. SERS spectral and optical images analysis

To investigate the topography and chemical composition of fine particles, we scanned the optical images and SERS spectra of 12 off-line samples (Fig. S1, Fig. 2), and selected 24–104 effective Raman spectra for every sample. To study changes in particle characteristics during the haze episode, among the particles, three representative samples were picked (Fig. 2), one before (Sample 1), one during (Sample 6), and one after the event (Sample 12). Before the haze event, based on the Raman optical images, predominantly opaque particles were observed (Fig. 2a1). Further spectral analysis illustrated that the characteristic peaks of these opaque particles were mainly at 1350 cm^{-1} (D-band) and 1589–1600 cm^{-1} (G-band) (Rosen and Novakov, 1977; Sze et al., 2001), which were assigned to soot, and represented a lattice defect and a perfect crystal form of crystalline graphite, respectively (Fig. 2b1). When $PM_{2.5}$ pol-

Table 1 – Parameters of individual $PM_{2.5}$ samples.

Sample	Date and Time	AQI	$PM_{2.5}$ (μg/m^3)	T (°C)	RH (%)	WS (km/hr)
1	9.5 14:00	25	3	30.1	18.1%	9
2	9.6 14:00	27	10	30.7	18.1%	6.48
3	9.7 21:00	151	116	28.3	57.1%	3.6
4	9.8 9:00	160	122	26.1	58.9%	2.52
5	9.8 14:00	161	123	32	41.2%	5.76
6	9.8 21:00	164	125	29	63.5%	9.36
7	9.9 9:00	128	97	24.2	71.7%	2.52
8	9.9 14:00	138	105	29	51.8%	3.24
9	9.9 21:00	86	59	28.1	56.8%	2.88
10	9.10 14:00	49	34	23.2	71.7%	2.52
11	9.10 21:00	61	44	23.3	66.6%	2.52
12	9.11 9:00	14	3	24.4	32.7%	9.36

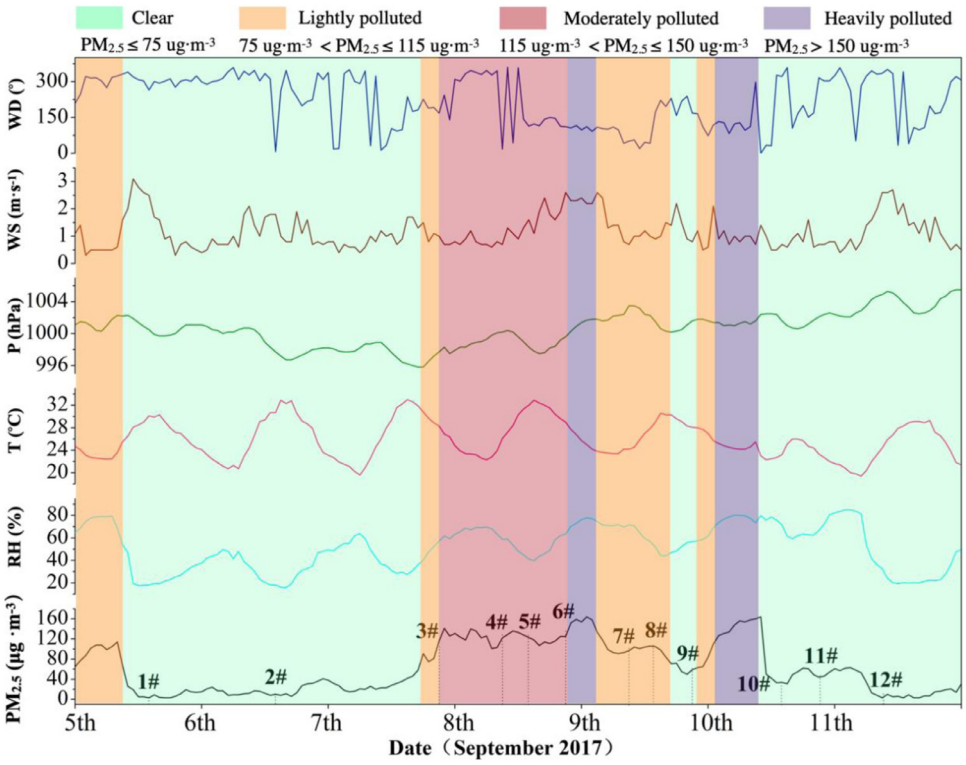

Fig. 1 – Temporal variations of $PM_{2.5}$, relative humidity (RH), temperature (T), pressure (P), wind speed (WS), and wind direction (WD) during the haze event from September 5 to 11 2017, in Beijing, China. The sampling period is marked green ($PM_{2.5} \leq 75$ μg/m^3, clear days), orange (75 μg/m^3 < $PM_{2.5} \leq 115$ μg/m^3, lightly polluted days), red (115 μg/m^{-3} < $PM_{2.5} \leq 150$ μg/m^{-3}, moderately polluted days), and purple (150 μg/m^3 < $PM_{2.5} \leq 250$ μg/m^3, heavily polluted days). The black dashed lines represent the collection times of the 12 individual particle samples during the haze episode.

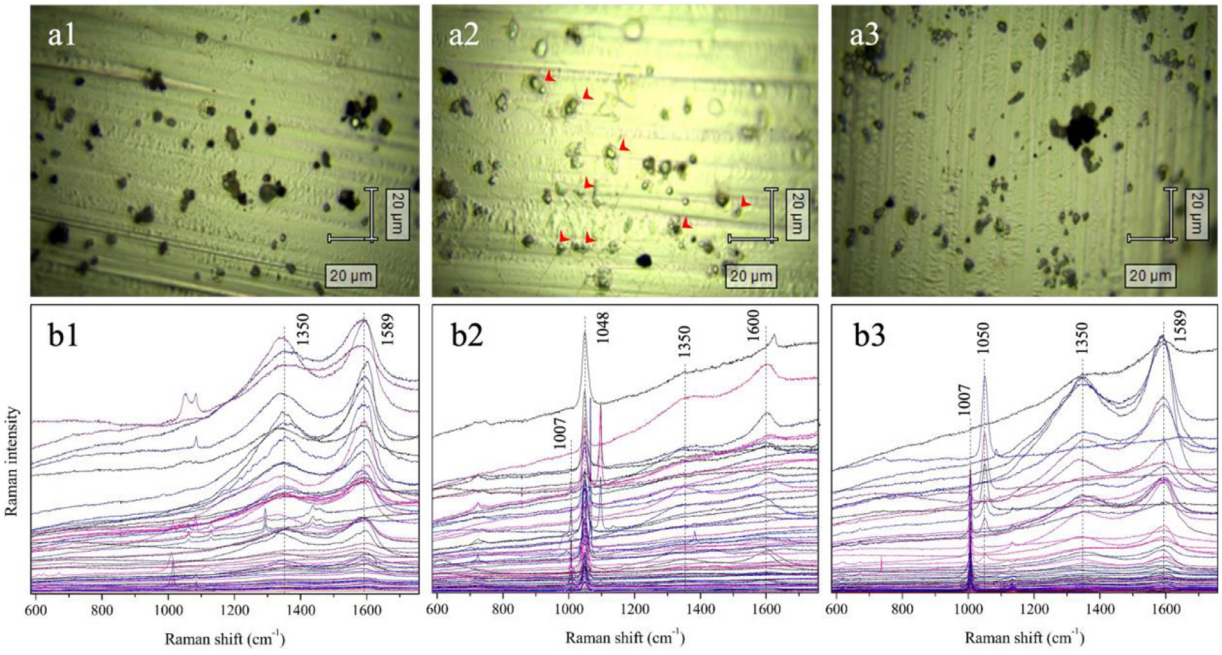

Fig. 2 – Surface-enhanced Raman scattering (SERS) spectrum corresponding to samples collected before, during, and after the haze event (1–3, respectively). (a1–a3) Raman optical images of $PM_{2.5}$ particles (red arrows in a2 indicate core-shell structures), and (b1–b3) SERS spectra of individual $PM_{2.5}$ particles.

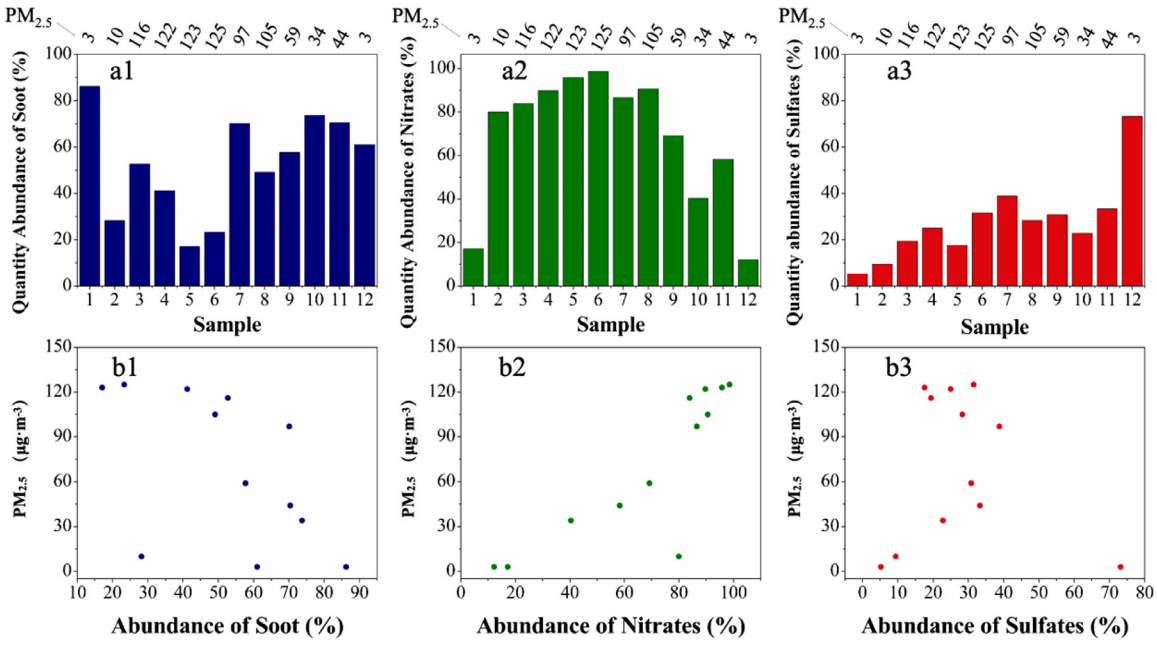

Fig. 3 – (a1–a3) Relative abundance of soot, nitrates, and sulfates during the haze event. (b1–b3) Relationship between $PM_{2.5}$ mass concentration and the abundance of soot, nitrates, and sulfates.

lution increased, the opaque material remained with a layer of transparent material surrounding them, forming a core-shell structure (red arrows in Fig. 2a2). According to spectral analysis, the opaque particles were still soot particles with their characteristic peaks mainly at 1350 and 1589–1600 cm^{-1}; the characteristic peaks corresponding to the transparent material were mainly at ~1007 and ~1045 cm^{-1}, which were assigned to sulfates and nitrates, respectively (Fig. 2b2) (Ling and Chan, 2007; Sun et al., 2019a). As the haze event dissipated, the particles became less transparent again, owing to the increased soot component and decreased sulfate and nitrate components (Fig. 2a3–b3). In conclusion, the $PM_{2.5}$ particles consisted of three main components: soot, nitrates, and sulfates. Soot existed in the form of opaque material and was more abundant on clear days. Nitrates and sulfates existed in the form of transparent material and were more abundant on hazy days.

2.2.2. *Quantity abundance analysis*

To conduct a more specific analysis of the relationship between the $PM_{2.5}$ pollution degree and the relative abundances of the three main $PM_{2.5}$ particle components (soot, nitrates, and sulfates), spectrum quantity statistics was performed using data corresponding to the 12 samples, and the characteristic peaks of every spectrum were analyzed (Fig. S2, Table 2). According to the SERS standard spectra, the characteristic peaks of the spectra, at 1350–1360 cm^{-1} (D-band) and 1580–1600 cm^{-1} (G-band), were assigned to soot. The characteristic peaks at 724, 1015, 1045, 1050, 1061, and 1066 cm^{-1} were assigned to nitrates; those at 608, 614, 620, 979, 1007, and 1129 cm^{-1} were assigned to sulfates (Sun et al., 2019a; Wang et al., 2011). In addition to soot, sulfates, and nitrates, there were a certain number of spectra assigned as unidentified characteristic peaks. These were concentrated at 618–635, 665–680, 1080-1097, 1290–1320, 1560–1570, and 1606–1655 cm^{-1}. We speculated that these peaks possibly belonged to SOA (Craig et al., 2015; Ofner et al., 2016).

Further relationship analysis showed that the average abundance of soot was 62.87% on clear days and 33.58% on moderately polluted days. Moreover, the average relative abundance of soot before and after the haze event was 1.5 times the value observed during the haze event. There was a reverse correlation between the abundance of soot and the $PM_{2.5}$ mass concentration (Fig. 3). However, the relative abundance of nitrates during the haze event (90.87%) was significantly greater than that before and after the event (46.22%), indicating that more nitrates were generated on hazy days. In addition, the proportion of sulfate increases slowly with increasing pollution.

2.2.3. *DCLS analysis*

To perform a major analysis of the abundance of the different components in the 12 collected samples, DCLS analysis was employed. The standard spectra of AS, AN, and GO, which were used to represent sulfates, nitrates, and soot, respectively, were input as reference spectra (Fig. S3). Then, we input the spectra of 12 offline samples to obtain compositional information for sulfates, nitrates, and soot in each sample (Fig. 4, Table S1).

The results indicate that before the haze event, soot was the most abundant $PM_{2.5}$ component in samples 1 and 2 (89.49% and 60.12%, respectively). As pollution increased, the abundance of sulfates remained almost unchanged, that of nitrates increased, and that of soot decreased; the lowest abundance of soot was 41.47 (sample 6). Next, the proportion of soot gradually increased as the $PM_{2.5}$ concentration decreased (Fig. 4a). The relative abundance of soot and the $PM_{2.5}$ concentration were inversely related ($R^2 = 0.50$, Fig. 4b). We specu-

Table 2 – Abundance analysis of the chemical components of $PM_{2.5}$ particles.

Sample	Number of effective spectra	Sulfates	Nitrates	Soot	Unidentified characteristic peaks
1	58	5.20%	17.20%	86.20%	25.90%
2	85	9.40%	80%	28.20%	11.80%
3	93	19.40%	83.90%	52.70%	11.80%
4	68	25%	89.70%	41.20%	17.60%
5	68	17.60%	95.80%	17.10%	29.40%
6	73	31.50%	98.60%	23.30%	11%
7	67	38.80%	86.60%	70.10%	13.4%
8	53	28.30%	90.60%	49.10%	20.80%
9	104	30.80%	69.20%	57.70%	30.80%
10	57	22.80%	40.40%	73.70%	22.80%
11	24	33.30%	58.30%	70.40%	16.70%
12	82	73.20%	12.20%	61%	40.20%

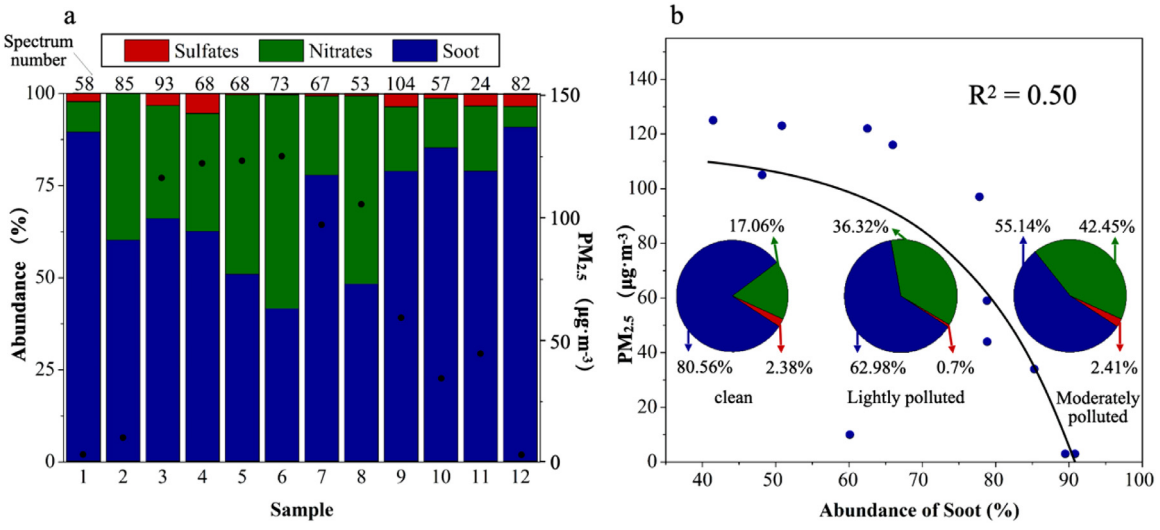

Fig. 4 – (a) Time series of the relative abundance of sulfates, nitrates, and soot during the haze event. (b) Relationship between $PM_{2.5}$ and the abundance of soot, nitrates, and sulfates on clear, lightly polluted, and moderately polluted days.

late that this is because during atmospheric aging, increasing RH brought about an increase in the sulfate and nitrate contents of the particles, decreasing the relative abundance of hydrophobic soot (Liu et al., 2017a; Sun et al., 2018; Xu et al., 2017). In addition, the results also indicate that soot was the most abundant component of the particles, with an average relative abundance of 69.18%, followed by nitrates (28.71%), and sulfates (2.11%). The relatively less abundance of nitrates and sulfates were also observed in online data (Table S2). Furthermore, we conducted pie analysis of the abundance of soot, nitrates, and sulfates on clear days, lightly polluted days, and moderately polluted days (Fig. 4b). The results illustrate that as $PM_{2.5}$ pollution increased, the abundance of soot decreased, that of nitrates increased, and that of sulfates showed no obvious change. DCLS was becoming a fast and effective way to obtain relative concentration information. However, due to the limitation of method principle, DCLS results were depended on reference spectra while not able to accommodate nonlinearities in the response (Zhang et al., 2005). In future research, we will combine a variety of powerful technologies to obtain more comprehensive information about the particle component. The quantity abundance analysis and DCLS analysis both provided abundant information regarding the chemical composition of the fine particles. They also provided theoretical support for developing haze prevention and control targets.

2.3. *Mixing state analysis*

To more intuitively explore the difference between the mixing states of the fine particles on clear and haze event days, Raman mapping analysis was performed (Fig. 5a1–e3 for clear days, Fig. 5a4–e6 for hazy days). Raman peaks in the ranges of 975–980, 1045–1050, 1350–1360, and 1580–1600 cm^{-1} represented sulfates (red in Fig. 5), nitrates (green in Fig. 5), the D-band (magenta in Fig. 5), and the G-band (blue in Fig. 5), respectively. On clear days, nitrates accounted for a majority of the fine particles, while sulfate abundance was relatively low. On hazy event days, the abundance of sulfates and nitrates increased and the signals corresponding to sulfates and nitrates partially overlapped. Further spectral analysis revealed that Raman peaks at 1045 and 1050 cm^{-1} coexisted on haze

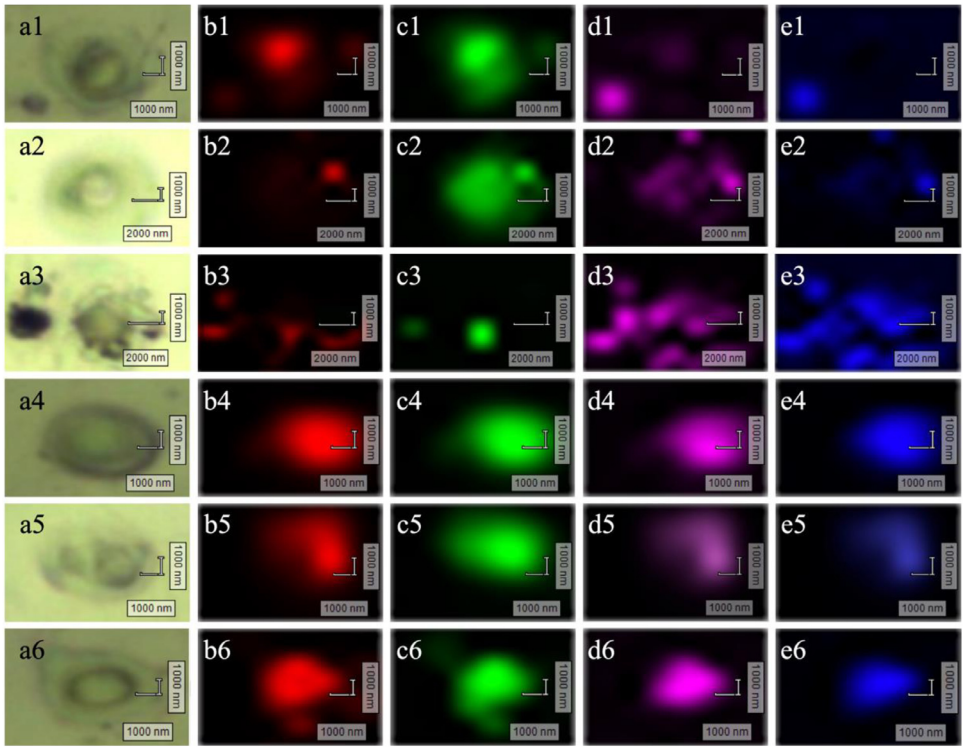

Fig. 5 – Mapping analysis of the mixing state of fine particles on clear days (a1–e3) and hazy days (a4–e6). (a) Raman optical image of fine particles and the Raman mapping signals of: (b) sulfates (red), (c) nitrates (green), (d) the D-band (magenta), and (e) the G-band (blue).

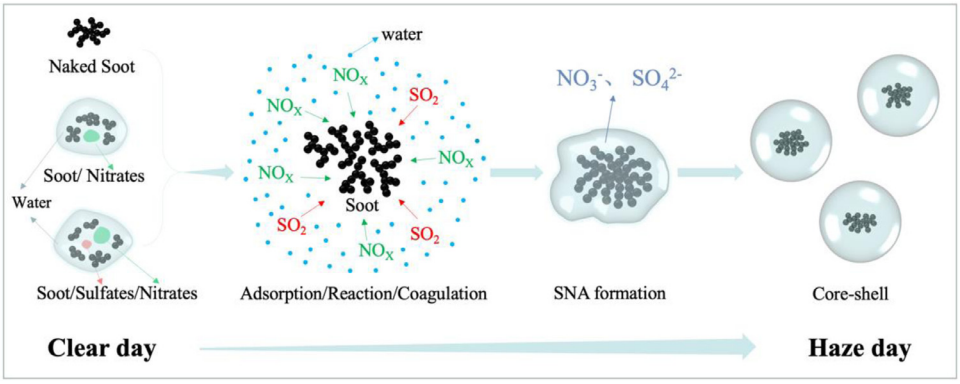

Fig. 6 – Conceptual graph showing the mechanism for the production of the core-shell structure of $PM_{2.5}$.

event days, indicating the formation of $2NH_4NO_3{\cdot}(NH_4)_2SO_4$ and $3NH_4NO_3{\cdot}(NH_4)_2SO_4$ (Ling and Chan, 2007; Sun et al., 2019b; Wang et al., 2011). This confirmed the internal mixing of sulfates and nitrates, in accordance with the mapping results. The location of soot within the fine particles changed from the edge on clear days to the center on hazy days, resulting in a core-shell structure with soot as the core and SNA as the shell.

We speculate that the mechanism for the production of this interesting phenomenon was as follows: on clear days, several types of particles mixed simply. There were freshly soot particles, and the different composition of soot, nitrates, and sulfates. Fresh soot existed in the form of hydrophobic chain spherules, whose irregular geometry and onion-like microstructure resulted in excellent adsorption performance (Fu et al., 2012; Zhang et al., 2008). During atmospheric aging, soot provided action sites on its surface that catalyzed the conversion of NO_X and SO_2 to nitrates and sulfates, respectively (Adachi et al., 2010; Han et al., 2013a, 2013b; He et al., 2018; Huang and Yu, 2008; Khalizov et al., 2010; Li et al., 2016b; Zhao et al., 2017). During this period, RH increased and hydrophilic nitrates and sulfates mixed internally and surrounded the soot, causing the original irregularly shaped particles to change to compact spherical particles (Fig. 6) (Ao et al., 2019; Li et al., 2017; Niu et al., 2012; Sarangi et al., 2019; Yuan et al., 2019). At this time, polluted fine particles collected,

forming a core-shell structure on the SERS sampling membranes, centered on soot (Fig. 5). Detailed mixture information on this core-shell structure could better explain the haze formation mechanism.

3. Conclusions

In this study, SERS was used to investigate the morphology, chemical composition, and mixing state of $PM_{2.5}$ particles during a haze episode. It was observed that the major components of $PM_{2.5}$ particles were soot, nitrates, and sulfates, with soot showing the highest relative abundance. Furthermore, a reverse correlation was observed between the abundance of soot and $PM_{2.5}$ mass concentration, which is because on hazy days, the former declined, while SNA concentration increased. We also observed that the polluted fine particles had an interesting core-shell structure, which can enhance understanding regarding the mechanism for the formation of haze. Our research results build on previous works conducted on the mixing states of particles, and can serve as the basis for policy formulation regarding haze prevention and control.

Acknowledgements

This work was supported by the National Natural Science Foundation of China (Nos. 21707077, 21775042), the National Key Research and Development Program of China (No. 2017YFA0207003), and the Fundamental Research Funds for the Central Universities (No. 2020 MS037).

Appendix A Supplementary data

Supplementary material associated with this article can be found, in the online version, at doi:10.1016/j.jes.2020.12.008.

REFERENCES

Adachi, K., Chung, S.H., Buseck, P.R., 2010. Shapes of soot aerosol particles and implications for their effects on climate. J. Geophys. Res. Atmos. 115.

Ao, J., Feng, Y., Wu, S., Wang, T., Ling, J., Zhang, L., et al., 2019. Rapid, 3D chemical profiling of individual atmospheric aerosols with stimulated raman scattering microscopy. Small Methods.

Ault, A.P., Axson, J.L., 2017. Atmospheric aerosol chemistry: spectroscopic and microscopic advances. Anal. Chem. 89, 430–452.

Craig, R.L., Bondy, A.L., Ault, A.P., 2015. Surface enhanced raman spectroscopy enables observations of previously undetectable secondary organic aerosol components at the individual particle level. Anal. Chem. 87, 7510–7514.

Dong, X., Ohnoutek, L., Yang, Y., Feng, Y., Wang, T., Tahir, M.A., et al., 2019. Cu/Ag sphere segment void array as efficient surface enhanced raman spectroscopy substrate for detecting individual atmospheric aerosol. Anal. Chem. 91, 13647–13657.

Fu, H., Chen, J., 2017. Formation, features and controlling strategies of severe haze-fog pollutions in China. Sci. Total Environ. 578, 121–138.

Fu, H., Zhang, M., Li, W., Chen, J., Wang, L., Quan, X., et al., 2012. Morphology, composition and mixing state of individual carbonaceous aerosol in urban Shanghai. Atmos. Chem. Phys. 12, 693–707.

Fu, Y., Kuppe, C., Valev, V.K., Fu, H., Zhang, L., Chen, J., 2017. Surface-enhanced raman spectroscopy: a facile and rapid method for the chemical component study of individual atmospheric aerosol. Environ. Sci. Technol. 51, 6260–6267.

Guo, S., Hu, M., Zamora, M.L., Peng, J., Shang, D., Zheng, J., et al., 2014. Elucidating severe urban haze formation in China. Proc. Natl. Acad. Sci. U.S.A. 111, 17373–17378.

Han, C., Liu, Y., He, H., 2013a. Heterogeneous photochemical aging of soot by NO_2 under simulated sunlight. Atmos. Environ. 64, 270–276.

Han, C., Liu, Y., He, H., 2013b. Role of organic carbon in heterogeneous reaction of NO_2 with soot. Environ. Sci. Technol. 47, 3174–3181.

He, G., Ma, J., He, H., 2018. Role of carbonaceous aerosols in catalyzing sulfate formation. ACS Catal 8, 3825–3832.

He, K., Yang, F., Ma, Y., Zhang, Q., Yao, X., Chan, C.K., et al., 2001. The characteristics of $PM_{2.5}$ in Beijing, China. Atmos. Environ. 35, 4959–4970.

Huang, X.F., Yu, J.Z., 2008. Size distributions of elemental carbon in the atmosphere of a coastal urban area in South China: characteristics, evolution processes, and implications for the mixing state. Atmos. Chem. Phys. 8, 5843–5853.

Khalizov, A.F., Cruz-Quinones, M., Zhang, R., 2010. Heterogeneous Reaction of NO_2 on fresh and coated soot surfaces. J. Phys. Chem. A. 114, 7516–7524.

Kulmala, M., 2015. China's choking cocktail. Nature 526, 497–499.

Li, K., Chen, L., Han, K., Lv, B., Bao, K., Wu, X., et al., 2017. Smog chamber study on aging of combustion soot in isoprene/SO_2/NOx system: Changes of mass, size, effective density, morphology and mixing state. Atmos. Res. 184, 139–148.

Li, W., Chi, J., Shi, Z., Wang, X., Chen, B., Wang, Y., et al., 2014a. Composition and hygroscopicity of aerosol particles at Mt. Lu in South China: Implications for acid precipitation. Atmos. Environ. 94, 626–636.

Li, W., Shao, L., Shi, Z., Chen, J., Yang, L., Yuan, Q., et al., 2014b. Mixing state and hygroscopicity of dust and haze particles before leaving Asian continent. J. Geophys. Res. Atmos. 119, 1044–1059.

Li, W., Shao, L., Zhang, D., Ro, C-U., Hu, M., Bi, X., et al., 2016a. A review of single aerosol particle studies in the atmosphere of East Asia: morphology, mixing state, source, and heterogeneous reactions. J. Clean. Prod. 112, 1330–1349.

Li, W., Shi, Z., Yan, C., Yang, L., Dong, C., Wang, W., 2013. Individual metal-bearing particles in a regional haze caused by firecracker and firework emissions. Sci. Total Environ. 443, 464–469.

Li, W., Sun, J., Xu, L., Shi, Z., Riemer, N., Sun, Y., et al., 2016b. A conceptual framework for mixing structures in individual aerosol particles. J. Geophys. Res. Atmos. 121, 13784–13798.

Ling, T.Y., Chan, C.K., 2007. Formation and transformation of metastable double salts from the crystallization of mixed ammonium nitrate and ammonium sulfate particles. Environ. Sci. Technol. 41, 8077–8083.

Liu, W., He, X., Pang, S., Zhang, Y., 2017a. Effect of relative humidity on O_3 and NO_2 oxidation of SO_2 on α-Al_2O_3 particles. Atmos. Environ. 167, 245–253.

Liu, W., Wang, H., Du, J., Jing, C., 2017b. Raman microspectroscopy of nucleus and cytoplasm for human colon cancer diagnosis. Biosens. Bioelectron. 97, 70–74.

Lu, Y., Chi, J., Yao, L., Yang, L., Li, W., Wang, Z., et al., 2015. Composition and mixing state of water soluble inorganic ions during hazy days in a background region of North China. Sci. China-Earth Sci. 58, 2026–2033.

Minutolo, P., Rusciano, G., Sgro, L.A., Pesce, G., Sasso, A., D'Anna, A., 2011. Surface enhanced Raman spectroscopy (SERS) of particles produced in premixed flame across soot threshold. Proc. Combust. Inst. 33, 649–657.
Niu, H., Shao, L., Zhang, D., 2012. Soot particles at an elevated site in eastern China during the passage of a strong cyclone. Sci. Total Environ. 430, 217–222.
Ofner, J., Deckert-Gaudig, T., Kamilli, K.A., Held, A., Lohninger, H., Deckert, V., et al., 2016. Tip-Enhanced Raman Spectroscopy of atmospherically relevant aerosol nanoparticles. Anal. Chem. 88, 9766–9772.
Riemer, N, Ault, A.P., West, M., Craig, R.L., Curtis, J.H., 2019. Aerosol mixing state: measurements, modeling, and impacts. Rev. Geophys. 57, 187–249.
Rosen, H., Novakov, T., 1977. Raman scattering and the characterisation of atmospheric aerosol particles. Nature 266, 708–710.
Sarangi, B., Ramachandran, S., Rajesh, T.A., Dhaker, V.K., 2019. Black carbon linked aerosol hygroscopic growth: Size and mixing state are crucial. Atmos. Environ. 200, 110–118.
Sun, J., Liu, L., Xu, L., Wang, Y., Wu, Z., Hu, M., et al., 2018. Key role of nitrate in phase transitions of urban particles: implications of important reactive surfaces for secondary aerosol formation. J. Geophys. Res. Atmos. 123, 1234–1243.
Sun, Z., Duan, F., He, K., Du, J., Yang, L., Li, H., et al., 2019a. Physicochemical analysis of individual atmospheric fine particles based on effective surface-enhanced Raman spectroscopy. J. Environ. Sci. 75, 388–395.
Sun, Z., Duan, F., He, K., Du, J., Zhu, L., 2019b. Sulfate-nitrate-ammonium as double salts in $PM_{2.5}$: Direct observations and implications for haze events. Sci. Total Environ. 647, 204–209.
Sze, S.K., Siddique, N., Sloan, J.J., Escribano, R., 2001. Raman spectroscopic characterization of carbonaceous aerosols. Atmos. Environ. 35, 561–568.
Tan, J., Duan, J., He, K., Ma, Y., Duan, F., Chen, Y., et al., 2009. Chemical characteristics of $PM_{2.5}$ during a typical haze episode in Guangzhou. J. Environ. Sci. 21, 774–781.
Vajna, B., Farkas, I., Szabo, A., Zsigmond, Z., Marosi, G., 2010. Raman microscopic evaluation of technology dependent structural differences in tablets containing imipramine model drug. J. Pharm. Biomed. Anal. 51, 30–38.
Wang, F., Zheng, Y., Zhang, Y., 2011. Temporally and spatially resolved investigation on the efflorescence process of a mixed droplet of ammonium sulfate and ammonium nitrate. Chin. Sci. Bull. 56, 2600–2603.
Wang, W., Shao, L., Xing, J., Li, J., Chang, L., Li, W., 2018. Physicochemical Characteristics of Individual Aerosol Particles during the 2015 China Victory Day Parade in Beijing. Atmosphere 9.
Wang, X., Chen, J., Cheng, T., Zhang, R., Wang, X., 2014. Particle number concentration, size distribution and chemical composition during haze and photochemical smog episodes in Shanghai. J. Environ. Sci. 26, 1894–1902.
Wang, X., Zhang, Y., Chen, H., Yang, X., Chen, J., Geng, F., 2009. Particulate nitrate formation in a highly polluted urban area: a case study by single-particle mass spectrometry in Shanghai. Environ. Sci. Technol. 43, 3061–3066.
Xu, L., Duan, F., He, K., Ma, Y., Zhu, L., Zheng, Y., et al., 2017. Characteristics of the secondary water-soluble ions in a typical autumn haze in Beijing. Environ. Pollut. 227, 296–305.
Yang, S., Duan, F., Ma, Y., Li, H., Ma, T., Zhu, L., et al., 2020. Mixed and intensive haze pollution during the transition period between autumn and winter in Beijing, China. Sci. Total Environ. 711, 134745.
Yuan, Q., Xu, J., Wang, Y., Zhang, X., Pang, Y., Liu, L., et al., 2019. Mixing State and Fractal Dimension of Soot Particles at a Remote Site in the Southeastern Tibetan Plateau. Environ. Sci. Technol. 53, 8227–8234.
Zhang, L., Henson, M.J., Sekulic, S.S., 2005. Multivariate data analysis for Raman imaging of a model pharmaceutical tablet. Anal. Chim. Acta. 545, 262–278.
Zhang, Q., Yan, R., Fan, J., Yu, S., Yang, W., Li, P., et al., 2015. A heavy haze episode in shanghai in december of 2013: characteristics, origins and implications. Aerosol Air Qual. Res 15, 1881–1893.
Zhang, R., Khalizov, A.F., Pagels, J., Zhang, D., Xue, H., McMurry, P.H., 2008. Variability in morphology, hygroscopicity, and optical properties of soot aerosols during atmospheric processing. Proc. Natl. Acad. Sci. U.S.A. 105, 10291–10296.
Zhao, Y., Liu, Y., Ma, J., Ma, Q., He, H., 2017. Heterogeneous reaction of SO_2 with soot: The roles of relative humidity and surface composition of soot in surface sulfate formation. Atmos. Environ. 152, 465–476.
Zhuang, X., Wang, Y., He, H., Liu, J., Wang, X., Zhu, T., et al., 2014. Haze insights and mitigation in China: an overview. J. Environ. Sci. 26, 2–12.